Heat Transfer Enhancement via Inhomogeneous Thermal Conductivity within Vertical Magnetohydrodynamic Ducts

C. J. Camobreco and G. J. Sheard

The Sheard Lab, Department of Mechanical and Aerospace Engineering
Monash University, Clayton, Victoria, 3800, Australia

Abstract

Inhomogeneous thermal conductivity disrupts the formation of the thermal boundary layer, increasing temperature gradients. This comes at the cost of reduced conducting area and natural convective velocities. However, at the low Prandtl numbers possessed by liquid metals (of order 10^{-2}), such as fusion reactor breeder fluids, the former outweighs the latter, and heat transfer can be promoted. Quasi-two-dimensional mixed convection simulations of a magnetohydrodynamic vertical duct were performed in the Rayleigh number and interaction parameter ranges of $10^2 < Ra < 10^4$ (with constant $Pr = 0.022$) and $100 < N < 1600$ respectively. Heat transfer enhancement was observed when buoyant forces (proportional to Ra) were sufficiently stronger than electromagnetic forces (proportional to N), which are imposed by the confining magnetic field.

Introduction

The magnetohydrodynamic (MHD) flow of a fusion reactor's electrically conducting breeder liquid, in the presence of its confining magnetic field, experiences a Lorentz force, $\vec{j} \times \vec{B}$, where $\vec{j}$ is the (induced) current density, and $\vec{B}$ the magnetic field. The Lorentz force restrains the flow, resulting in a uniform, slug flow profile [13]. The Lorentz force is also highly anisotropic [3] which suppresses turbulent mixing, to the detriment of heat transfer. These exacting conditions necessitate the use of heat transfer promoters. Hence, the aim of this work is to highlight an alternate means of enhancing heat transfer, which does not interfere with the flow of the breeder liquid through the duct. Furthermore, the Lorentz force diffuses momentum along the magnetic field direction (a relic of Alfvén wave propagation [19]), such that the global Joule dissipation is minimized [4]. Under the strong confining magnetic field the flow approaches two-dimensionality, except within the thin Hartmann boundary layers which form on walls perpendicular to the magnetic field. Hence, by invoking a quasi two-dimensional model, we are able to expediently analyse the dependence of velocity on key imposed parameters, including the Rayleigh number and interaction parameter.

The flow is considered to be quasi-two dimensional so long as momentum outside the Hartmann layers is able to diffuse within the whole core flow at timescales smaller than that of viscosity or inertia [15]. This diffusion timescale is sufficiently small if $Ha \gg 1$ and $N \gg 1$, where the Hartmann number, $Ha = aB(\sigma/\rho_0\nu)^{1/2}$, represents the ratio of the square of electromagnetic to viscous forces, and the interaction parameter, $N = Ha^2/Re$, represents the ratio of electromagnetic to inertial forces. Additionally the Reynolds number, $Re = U_0 L_c/\nu$, should also be much greater than unity, such that interaction between transverse planes is limited [19]. Note that a is the distance between two Hartmann walls, B the uniform magnetic field strength, U_0 a reference velocity, L_c the characteristic length (half the duct height, L_d) and σ, ρ_0 and ν the fluid's electrical conductivity, reference density and kinematic viscosity, respectively. In addition, $\vec{B}$ is considered to be imposed (no magnetic field component is induced by $\vec{u}$), hence the magnetic field is (quasi) static. This requires a small magnetic Reynolds number, $Re_m = U_0 L_c/\eta_m$, such that magnetic diffusion (where η_m is the magnetic diffusivity) dominates advection. These assumptions form the core of the SM82 model (developed by Sommeria and Moreau [19]), which is used within this work.

A great deal of research has been performed to validate the SM82 model, however, only three assumptions are pertinent to discuss, see [8, 12, 16] for more. Firstly, within Shercliff layers (which form on walls parallel to the magnetic field) viscosity acts at a similar timescale to electromagnetic diffusion [15], maintaining three-dimensional flows, inducing a 10% modelling error [17]. Secondly, the Hartmann layers must remain laminar and stable, such that viscous frictional forces, due to the no-slip condition, are conferred to the core by a linear Hartmann braking term [19]. This term takes the form H/Re in the momentum equation, where $H = n(L_c/a)^2 Ha$, is the Hartmann friction parameter, which considers geometric effects (where the number of Hartmann walls, $n = 2$). The ratio Re/Ha must remain below a critical value, which for transition is expected to be between 350 and 400 [10, 11]. Stability criteria are much higher [15]. A value of $Re/Ha = 1$ was used for all simulations. Thirdly, as mixed convection is simulated, the criteria, $Gr < Ha^4/N_b^2$, governing the strength of buoyant to electromagnetic forces, should be enforced. For Q2D to be achieved, $N_b \geq 4$ [2], where N_b represents a buoyant core interaction parameter, and the Grashof number, $Gr = g\beta\Delta\hat{\theta}L_c^3/\nu^2$, indicates the relative strength of buoyant to viscous forces (note $Ra = GrPr$). Additionally g is the acceleration due to Earth's gravity, $\Delta\hat{\theta}$ a dimensional temperature increment and β the fluid's volumetric thermal expansion coefficient.

Methodology

A periodic duct section is modelled (see Figure 1). Periodicity requires that the effect of the background horizontal thermal gradient be sufficiently less than that of thermal fluctuations, or $\Lambda/PrReU \ll 1$, where $\Lambda = n_s L_s/L_d$ is the conducting length fraction (a conducting area fraction if not Q2D), n_s the total number of conducting sections (along L_d), L_s the length of a conducting section and U the area flow rate. Nodes on the periodic boundaries (inlet and outlet) are then considered to have identical fluctuating velocity, temperature and pressure values. All other walls have the no-slip condition imposed, and perfect electrical and thermal insulation, except for the conducting sections of the heated face. The uniform imposed magnetic field is aligned with the transverse (z) direction, with the x-y plane simulated. The initial velocity field defined was the analytic, fully developed profile [15]. Relative temperatures were always used. The pressure drop is scaled at each timestep to maintain a constant flow rate. The fluid is incompressible, Newtonian and electrically conducting. With the exception of density (modelled via the Boussinesq approximation) all fluid properties are assumed constant.

Use of the Boussinesq approximation for buoyancy, where the density is linearly related to the reference density by the dif-

ference in relative temperatures, $\rho/\rho_0 = 1 - \beta\left(\hat{\theta} - \hat{\theta}_0\right)$, is arguably contentious. The Boussinesq approximation holds only for small temperature gradients, which is not the case within fusion reactor blankets, where temperature differences are expected to be 250 °C [1] to 300 °C [5]. However, qualitatively similar results should still be obtained [20], although quantitative discrepancies (of up to 10%) may be observed [6, 14]. Within a square cavity, at $Ha = 100$, the error in applying the Boussinesq approximation remains small when considering the average Nusselt number (2%), but large differences in peak Nusselt numbers and velocities (up to 20%) were observed, for Ra up to 10^6 [7]. Hence, the Boussinesq approximation still appears appropriate, as low Rayleigh numbers ($Ra < 10^4$) were simulated, and since the approximation is used in most other MHD research [20].
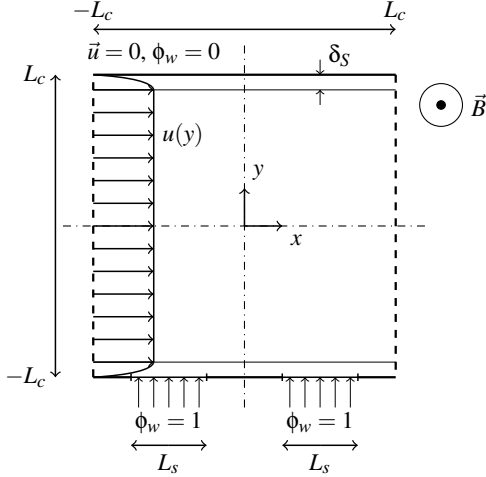
Figure 1: Schematic diagram of the system. The periodic boundaries are denoted by thick dashed lines. The length over which a constant heat flux is imposed, L_s and the orientation of gravity (not shown), relative to that of the forced flow, are varied. In the absence of natural convection the velocity profile will have an appearance similar to $u(y)$, approximately flat within the core region, and decaying to the no-slip condition within the Shercliff layers, each of thickness δ_S.

The governing Q2D equations, in non-dimensional form, are

$$\vec{\nabla} \cdot \vec{u} = 0, \tag{1}$$

$$\frac{\partial \vec{u}}{\partial t} + (\vec{u} \cdot \vec{\nabla})\vec{u} = -\vec{\nabla}p + \frac{1}{Re}\nabla^2\vec{u} - \frac{H}{Re}\vec{u} - \vec{e}_y\frac{Ra}{Re^2Pr}\theta', \tag{2}$$

$$\frac{\partial \theta'}{\partial t} + \left(u\frac{\partial \theta'}{\partial x} + v\frac{\partial \theta'}{\partial y}\right) + \frac{\Lambda}{PrReU}u = \frac{1}{PrRe}\nabla^2\theta', \tag{3}$$

noting that $\vec{u} = (u, v)$ represents the Q2D velocity vector. The following scalings were used for non-dimensionalization: length (x or y) by L_c, time by L_c/U_0, velocity (u or v) by U_0, the differential operator by $1/L_c$, kinematic pressure by $\rho_0 U_0^2$ and temperature by a temperature increment $\Delta\hat{\theta}$, based on the heat flux imposed over one characteristic length ($\Delta\hat{\theta} = \hat{q}_wL_c/\alpha\rho_0C_p$). The domain was discretized with a macro element distribution, over which high polynomial order ($N_P = 10$) basis functions were employed. An in-house spectral element solver recasts the equations in a weak (integral) form using the Galerkin (weighted residual) method, and then solves the resulting set of ordinary differential equations. A three-step operator splitting scheme based on backwards differentiation is used for time integration [18].

The rate of heat transfer is quantified via the Nusselt number, $Nu = L_d^{-1}\int_{-L_c}^{L_c}2/(\theta'_b - \theta'_w)\mathrm{d}x$, where $\theta'_b = \int_{-L_c}^{L_c}uT\mathrm{d}y/\int_{-L_c}^{L_c}u\mathrm{d}y$ is the bulk fluctuating temperature and θ'_w the wall fluctuating temperature. The Nusselt number represents the ratio of convective heat transfer (T advected by u) to conduction from heated sections of the wall. As the bulk temperature depends on the streamwise velocity, it can be higher than (or equal to) the wall temperature while heat is still transferred from the wall. This will occur when a section of the flow reverses in the vicinity of the heated wall (the flow rate remains constant as the fluid further from the wall also accelerates in the opposite direction, creating an 'S-shaped' velocity profile). Regardless, the Nusselt number still indicates the degree of improvement in heat transfer, and when negative indicates that more thermal energy is carried in the direction opposite the forcing. Furthermore, a Nusselt number ratio, $Nu_R = Nu|_{\Lambda<1}/Nu|_{\Lambda=1}$, is used to compare the heat transfer rate for the modified ($\Lambda < 1$) duct to that of the unmodified ($\Lambda = 1$) duct, at the same N and Ra conditions.

Convergence Study

All simulations reached a time independent state, after which the maximum change in streamwise velocity was below 10^{-9}, and the change in spatially averaged Nusselt number less than 10^{-6} (10^{-7} for convergence testing). The most stringent set of conditions, $N = 200$ and $Ra = 10^4$, with $\Lambda = 0.5$, were used to test the sensitivity of Nu to the macro element distribution and polynomial resolution, as shown in Figure 2. Excellent convergence behaviour is observed (note the scale on the axis).
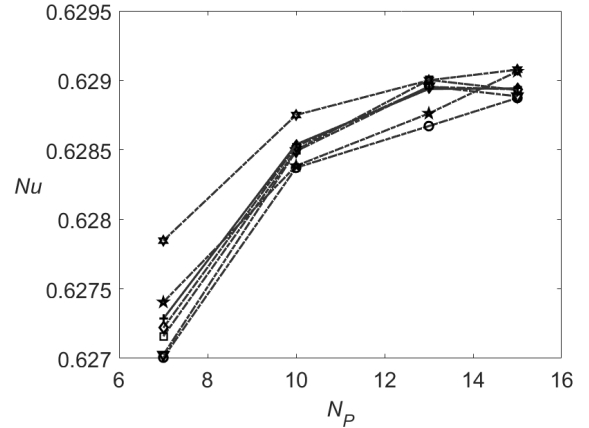
Figure 2: A plot of spatially averaged Nusselt number against polynomial order for various meshes, depicting 'hp' convergence, at $N = 200$, $Ra = 10^4$, $\Lambda = 0.5$, flow directed with gravity. The markers indicate meshes with the following numbers of elements: [1200, 1280, 1600, 1920, 2000, 2200, 2400] as [$\bigcirc$, $\triangledown$, $\square$, $\diamond$, $\star$, $+$, $\maltese$]; the 2200 element mesh is used hereafter.

However, the convergence behaviour is slightly impacted by the discontinuous change in thermal boundary condition. This introduces small 'wiggles' into the interpolating polynomial, as the Galerkin method only weakly enforces Neumann boundary conditions [9]. The average heat flux ($L_s^{-1}\int_{-L_s}^{L_s}\phi_w(x)\mathrm{d}x$) was computed, for each simulation, to quantify this error, and always remained within 0.85% of $\phi_w = -1$. In addition the tolerance for Nusselt number calculations (both in y when computing θ'_b and in x for spatial averaging) was maintained at 10^{-4}.

Results

Two regimes are present within the range of simulated condi-

tions, determined by the relative velocity contributions due to forced and natural convection. When Ra is small and N large, the flow is forcing dominated, with a 'U-shaped' velocity profile, similar in appearance to that depicted in Figure 1. When Ra is large and N small, natural convection is dominant (or at least relevant), and the velocity profile tends to that of an 'S-shape', with reversed flow near the heated wall (where buoyancy is strongest). Varying the conducting length fraction, Λ, has a markedly different effect within these regimes. When the flow is forcing dominated, the flow velocity is virtually invariant with changes in Λ, and hence the convective capacity of the flow remains unchanged. However, when the imposed conditions allow the flow to reverse, the natural convective velocity is found to be proportional to $Ra^{1\pm1E-8}\Lambda^{1\pm1E-8}N^{-1.835\mp0.002}$. The linear scaling with Λ indicates that as Λ is reduced, natural convective forces become weaker, and the forced ('U-shaped') profile will eventually return. Hence, at low Λ the flow will have limited convective capacity for heat transfer, as for a forced flow, and increasing Λ will provide further increases to convective heat transport, which is highest at the unmodified $\Lambda = 1$ condition.

However, the reason for reducing Λ is to improve thermal gradients at the wall, by disrupting the formation of the thermal boundary layer. The normalised temperature gradient (ψ_w) was calculated at the centre of each conducting section (with normalising through $\Theta'_w = (\theta' - \theta'_c)/(\theta'_h - \theta'_c)$, where θ'_h and θ'_c represents the fluctuating temperatures at the heated and insulated walls). The normalised temperature gradient was found to scale with the power law $\psi_w = \psi_w|_{\Lambda=1}\Lambda^{D_1}$ ($R^2 > 0.999$), where the constant exhibited minor variation with N within $-0.837 < D_1 < -0.739$. The scaling was effectively invariant of Ra and flow direction. Hence, reducing Λ greatly increases temperature gradients at the wall, at all duct conditions, improving the efficiency of conduction. Therefore, heat transfer is able to be promoted if the improvements in conduction efficiency are not outweighed by the reductions in the flow's capacity to convect heat.
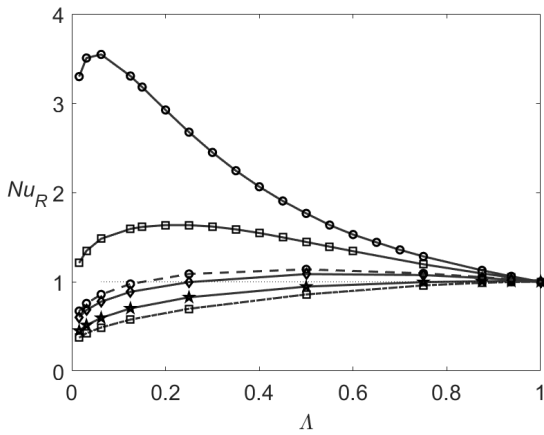
Figure 3: A plot of Nusselt number ratio against conducting length fraction for flows directed with gravity. Variations in duct conditions are displayed as $N = [100, 200, 400, 800, 1600]$ with markers [$\bigcirc$, $\square$, $\diamond$, $\star$, φ] and $Ra = [10^2, 10^3, 10^4]$ with lines [$-\cdot$, $--$, $-$] (some are omitted for clarity).

The effect of the improvements to normalised temperature gradient are most clearly depicted within the forcing dominated regime. Within this regime, the convective capacity of the flow does not noticeably vary, hence the Nu_R curves scale as $Nu_R = Nu_R|_{\Lambda=1}\Lambda^{D_1+1}$ ($R^2 > 0.995$), as only the temperature

gradients and conducting area (proportional to Λ) are relevant. Two curves within the forcing dominated regime (at $Ra = 10^2$, $N = 200$ and $Ra = 10^4$, $N = 800$) are depicted in Figure 3, and all other forcing dominated conditions fall between these. Hence, within the forcing dominated regime, heat transfer is never promoted ($Nu_R < 1$) for all reductions in Λ. When the strength of natural convection increases, such that the forced, 'U-shaped' velocity profile is significantly deformed (but the flow has not reversed), the curves are very similar, and minimal heat transfer enhancement may occur. However, these conditions, as well as those when natural convection is dominant, indicate that a similar form of power law is obtained to the left of the peak. This is considered to be a regime where the flow still has limited convective transport (very low velocities, although with noticeable variation with Λ), and where enhancements in heat transfer are driven by improvements to the efficiency of conduction. Power law fits are also accurately obtained to the right of the peak, although with the opposite curvature when natural convection is dominant, hence the thermal boundary layer thickness is still driving changes in the efficiency of conduction, as velocity and area are linear with Λ. However, the fluid now has ample convective velocity but is conduction limited, as Λ is too large. Hence, matching the rates of convection and conduction provides the optimal rate of heat transfer, with lower Λ convection limited, and higher Λ conduction limited. The peak enhancement was obtained when natural convection was strongest ($Ra = 10^4$, $N = 100$), with $Nu_R = 3.546$ obtained at $\Lambda = 0.0625$. Furthermore, although the location of the peak appears to shift greatly, the flow rate within the jet adjacent to the heated wall is similar for all cases, between $0.005 < U_A < 0.437$. This indicates that although the peak heat transfer is obtained once the flow reverses (an 'S-shaped' profile), it is not necessary for heat transfer to be enhanced.
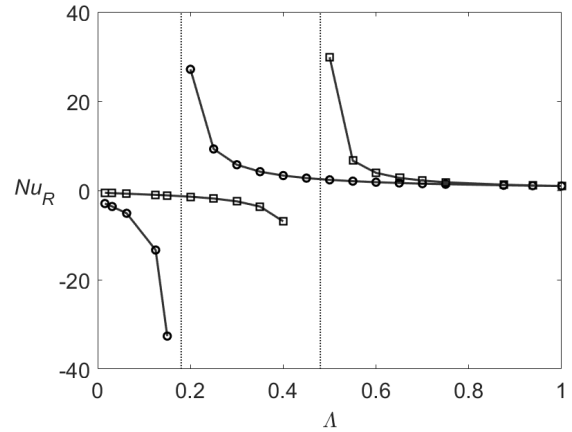
Figure 4: A plot of Nusselt number ratio against conducting length fraction for flows directed against gravity. Variations in duct conditions are displayed as $N = [100, 200, 400, 800, 1600]$ with markers [$\bigcirc$, $\square$, $\diamond$, $\star$, φ] and $Ra = [10^2, 10^3, 10^4]$ with lines [$-\cdot$, $--$, $-$]. The dotted lines are guides for the locations of the asymptotes where $\theta'_b = \theta'_w$.

When the flow conditions are forcing dominated the orientation of the flow with respect to gravity has little effect on heat transfer (the minimal improvement or reduction is symmetric about that for a horizontal duct). However, when natural convection is dominant, the appearance of the Nu_R curves, depicted in Figure 4, differ significantly. Firstly, when the flow is directed against gravity, and buoyancy aids the forced profile near the wall, the bulk temperature can reach the wall temperature value

(hence $Nu \to \infty$). This never occurs for flow directed with gravity as the forcing acts against buoyancy. However, this should be thought of as obtaining an "optimal" velocity profile, where the heat transported by the fluid is exactly that supplied by the wall, hence heat transfer cannot be further increased. However, at conditions close to this value, heat transfer enhancement is still being provided by improved temperature gradients, which act to bring θ'_b closer to θ'_w. Secondly negative Nu are obtained when the flow forms an 'S-shaped' profile (large Λ, when $\theta'_b > \theta'_w$), indicating that more heat is convected in the opposite direction to the driving pressure gradient. However, these appear as positive Nu_R when divided by $Nu|_{\Lambda=1}$, which must also be negative if some $Nu|_{\Lambda<1}$ are. Note in any case where the flow reverses, some of the bulk temperature cancels, and hence the Nu represents the net heat convected.

Conclusions

Reducing the conduction length fraction is shown to provide large increases in normalised temperature gradient at the wall. This scaled as a power law with the form $\psi_w = \psi_w|_{\Lambda=1}\Lambda_1^D$ ($-0.837 < D_1 < -0.739$), which indicates the effect of the conducting length fraction on thermal boundary layer development. This defines the correlation for the Nusselt number at forcing dominated conditions, which scale with Λ^{D_1+1}, and always results in reductions in heat transfer with decreasing Λ. These conditions are considered to be convection limited, due to low streamwise velocities. Even small increases in streamwise velocity, driven by natural convection (indicated in the flow rate within the adjacent jet, U_A), can provide large increases in heat transfer, with a definite peak of $Nu_R = 3.5460$ ($U_A = 0.4372$) obtained at $\Lambda = 0.0625$, $N = 100$ and $Ra = 10^4$. Further increases in Λ cause corresponding linear increases in the natural convective velocity (which scaled as $Ra\Lambda N^{-1.835}$). However, the flow then becomes conduction limited as the thermal boundary layer is not sufficiently disrupted. These regions are also relevant when the flow direction is reversed (against gravity), although the asymptotic behaviour exhibited does not allow this to be observed.

Acknowledgements

References

[1] Abdou, M., Morley, N. B., Smolentsev, S., Ying, A., Malang, S., Rowcliffe, A. and Ulrickson, M., Blanket/first wall challenges and required R&D on the pathway to DEMO, *Fusion Engineering and Design*, **100**, 2015, 2–43.

[2] Authié, G., Tagawa, T. and Moreau, R., Buoyant flow in long vertical enclosures in the presence of a strong horizontal magnetic field. Part 2. Finite enclosures, *European Journal of Mechanics B/Fluids*, **22**, 2003, 203–220.

[3] Burr, U., Barleon, L., Müller, U. and Tsinober, A., Turbulent transport of momentum and heat in magnetohydrodynamic rectangular duct flow with strong sidewall jets, *Journal of Fluid Mechanics*, **406**, 2000, 247–279.

[4] Davidson, P. A., Magnetic damping of jets and vortices, *Journal of Fluid Mechanics*, **299**, 1995, 153–186.

[5] de les Valls, E. M., Batet, L., de Medina, V., Fradera, J. and Sedano, L. A., Qualification of MHD effects in dual-coolant DEMO blanket and approaches to their modelling, *Fusion Engineering and Design*, **86**, 2011, 2326–2329.

[6] Gray, D. D. and Giorgini, A., The validity of the Boussinesq approximation for liquids and gases, *International Journal of Heat and Mass Transfer*, **19**, 1976, 545–551.

[7] Hosseinizadeh, S. F., Hajibagheri, M., Heidarnataj, M., Darbandi, M. and Javaherdeh, K., High gradient temperature thermo-buoyant flow in a square cavity with magnetoconvection using a novel non-Boussinesq algorithm, *Numerical Heat Transfer, Part A: Applications*, **64**, 2013, 255–272.

[8] Kanaris, N., Albets, X., Grigoriadis, D. and Kassinos, S., Three-dimensional numerical simulations of magnetohydrodynamic flow around a confined circular cylinder under low, moderate, and strong magnetic fields, *Physics of Fluids*, **25**, 2013, 074102.

[9] Karniadakis, G. E. and Sherwin, S. J., *Spectral/hp element methods for computational fluid dynamics*, Oxford University Press, 2005.

[10] Krasnov, D. S., Zienicke, E., Zikanov, O., Boeck, T. and Thess, A., Numerical study of the instability of the hartmann layer, *Journal of Fluid Mechanics*, **504**, 2004, 183–211.

[11] Moresco, P. and Alboussiére, T., Experimental study of the instability of the hartmann layer, *Journal of Fluid Mechanics*, **504**, 2004, 167–181.

[12] Mück, B., Günther, C., Müller, U. and Bühler, L., Three-dimensional MHD flows in rectangular ducts with internal obstacles, *Journal of Fluid Mechanics*, **418**, 2000, 265–295.

[13] Müller, U. and Bühler, L., *Magnetofluiddynamics in Channels and Containers*, Springer-Verlag Berlin Heidelberg, 2001.

[14] Ni, W., Qui, S., Su, G., Tian, W. and Wu, Y., Numerical investigation of buoyant effect on flow and heat transfer of Lithium-Lead Eutectic in DFLL-TBM, *Progress in Nuclear Energy*, **58**, 2012, 108–115.

[15] Pothérat, A., Quasi-two-dimensional perturbations in duct flows under transverse magnetic field, *Physics of Fluids*, **19**, 2007, 074104.

[16] Pothérat, A. and Kornet, K., The decay of wall-bounded MHD turbulence at low *rm*, *Journal of Fluid Mechanics*, **783**, 2015, 605–636.

[17] Pothérat, A., Sommeria, J. and Moreau, R., An effective two-dimensional model for MHD flows with a transverse magnetic field, *Journal of Fluid Mechanics*, **424**, 2000, 75–100.

[18] Sheard, G. J., *Viper, spectral-element flow solver*, 2009.

[19] Sommeria, J. and Moreau, R., Why, how, and when, MHD turbulence becomes two-dimensional, *Journal of Fluid Mechanics*, **118**, 1982, 507–518.

[20] Zhang, X. and Zikanov, O., Two-dimensional turbulent convection in a toroidal duct of a liquid metal blanket of a fusion reactor, *Journal of Fluid Mechanics*, **779**, 2015, 36–52.